INTERFACE

rsif.royalsocietypublishing.org

Research

Cite this article: Paoletti P, Jones GW, Mahadevan L. 2017 Grasping with a soft glove: intrinsic impedance control in pneumatic actuators. *J. R. Soc. Interface* **14**: 20160867. http://dx.doi.org/10.1098/rsif.2016.0867

Received: 29 October 2016
Accepted: 7 February 2017

Subject Category:
Life Sciences–Engineering interface

Subject Areas:
bioengineering, biomechanics, biomimetics

Keywords:
soft robotics, grasping, impedance control, bioinspired design

Author for correspondence:
L. Mahadevan
e-mail: lm@seas.harvard.edu

Electronic supplementary material is available online at https://doi.org/10.6084/m9.figshare.c.3694465

THE ROYAL SOCIETY PUBLISHING

Grasping with a soft glove: intrinsic impedance control in pneumatic actuators

P. Paoletti[1], G. W. Jones[2] and L. Mahadevan[3,4,5,6]

[1]School of Engineering, University of Liverpool, Liverpool L69 3GH, UK
[2]School of Mathematics, University of Manchester, Manchester M13 9PL, UK
[3]Paulson School of Engineering and Applied Sciences, [4]Department of Physics, [5]Wyss Institute for Biologically Inspired Engineering and [6]Kavli Institute for NanoBio Science and Technology, Harvard University, Cambridge, MA 02138, USA

PP, 0000-0001-6131-0377; GWJ, 0000-0001-6218-0367; LM, 0000-0002-5114-0519

The interaction of a robotic manipulator with unknown soft objects represents a significant challenge for traditional robotic platforms because of the difficulty in controlling the grasping force between a soft object and a stiff manipulator. Soft robotic actuators inspired by elephant trunks, octopus limbs and muscular hydrostats are suggestive of ways to overcome this fundamental difficulty. In particular, the large intrinsic compliance of soft manipulators such as 'pneu-nets'—pneumatically actuated elastomeric structures—makes them ideal for applications that require interactions with an uncertain mechanical and geometrical environment. Using a simple theoretical model, we show how the geometric and material nonlinearities inherent in the passive mechanical response of such devices can be used to grasp soft objects using force control, and stiff objects using position control, without any need for active sensing or feedback control. Our study is suggestive of a general principle for designing actuators with autonomous intrinsic impedance control.

1. Introduction

Complex haptic interaction with the world is a common task that many organisms successfully master. Indeed, humans and animals, with elephants and cephalopods being particularly spectacular examples, routinely use multifunctional soft limbs and appendages to safely interact with uncertain mechanical environments. Attempts to imitate this performance in artificial systems such as robotic grippers has highlighted the intrinsic difficulties associated with this task. These difficulties include the ability to get a good grasp on objects with different shapes while controlling the interaction force to achieve robust grasping without damaging the object (or the gripper itself) and simultaneously predicting the mechanical response of the unknown grasped objects [1].

The traditional approach to robotic manipulation is based on the active feedback control of hand-like grippers—composed of actuated rigid links and equipped with sensors and controllers to safely interact with the environment. Although techniques for the controlled motion of manipulators in the absence of obstacles or interacting with known objects are well established, both the stability of the system while in contact with objects of unknown stiffness and the safety of the manipulator and the object being held still pose significant challenges [1]. To see this, we note that, in the simplest setting where a rigid single degree-of-freedom actuator enters into contact with an elastic object with intrinsic stiffness k_e, the interaction force simply reads $k_e\Delta x$, where Δx is the indentation. This force can attain large values and can even destabilize a controller designed only to regulate the position of the end effector [1]. Embedding soft linkages in underactuated grippers can mitigate this issue by partially delegating the stabilization of the grasping task to the mechanical response of the gripper itself: see [2] for a recent design of an underactuated compliant grasper exploiting this principle; however, there are clear limitations to this approach, which requires partial or complete knowledge of the environment.

To partially circumvent the need for active sensing and feedback, a natural strategy is for the controller to emulate a dynamic relation between the

manipulator end-effector position and force, rather than merely controlling one of these variables. One of the first systematic frameworks for artificial grippers to move in this direction was proposed in a seminal paper by Hogan over 30 years ago [3], and it is commonly known as *impedance control*. In this scenario, stability is achieved by controlling the gripper dynamics, so that it emulates a dynamical impedance. In the context of the simple example from the previous paragraph, the dynamic impedance may be modelled by a virtual spring k_p, so that the interaction force now reads $k_p k_e (k_p + k_e)^{-1} \Delta x$. By choosing $k_p \ll k_e$, the interaction force can be greatly reduced and the overall closed-loop stability is preserved, albeit at the expense of an error in tracking the position of the end effector. This approach has since been extended and widely used to control the motion of robotic arms and fingers and, simultaneously, the force exerted on the grasped object, as reviewed for example in [1]. In modern implementations, a combination of position and force controllers is therefore used to divide the control task into subtasks normal and tangential to the contact surface [1]; examples of real experimental realizations of this class of controllers are presented in [4–6].

In all the approaches described above, the ability to predict the mechanical response of the grasped object and sense the position of the end effector is critical, but such information is not always available *a priori*. Therefore, the application of such techniques is limited to environments where the grasped objects are more or less homogeneous. Bio-inspired designs based on using soft materials are now emerging to circumvent the intrinsic limitations of traditional rigid robotic manipulators. These designs have many applications, including grasping, locomotion and surgery assistive devices [7–10], by using finger-like digits combined with either a learning phase that can be used to achieve stable grasping [11] or compliant joints that also achieve the same end without learning [12], or, at another extreme, a transition between fluid and rigid states in a confined granular medium achieved via a jamming transition [13]. Similarly, soft actuators inspired by muscular hydrostats—segmented tubular structures seen in a range of biological organs and organisms [14] that work by using a combination of muscles and hydraulics to generate and control both organ shape and the forces applied by it—are increasingly being used in soft robotics [15,16] as they minimize the computational and sensing resources for a robust interaction with an uncertain mechanical environment.

These examples suggest that soft robots that use highly compliant structural elements in their design are well placed as potential impedance-controlled manipulators. A particularly interesting class of these compliant structural elements are pneu-nets, a novel, simple and inexpensive design fabricated through soft lithography and capable of sophisticated motions with simple pneumatic inputs [17–19]. These soft limb or trunk-like elements are made of elastomeric silicone rubbers, which are flexible, exhibit high surface compliance and tolerate large tensile strains. This makes them particularly useful for handling soft or fragile objects, a daunting task for traditional hard manipulators. In fact, one can successfully complete such manipulating tasks in open loop, i.e. without using any active feedback control [17]. Despite these successes, a crucial limiting factor preventing a full exploitation of these concepts is the dearth of models with good predictive capabilities for actuator dynamics and the interaction force with the environment [9,10], which prevents further optimization of their design and their efficiency as grippers.

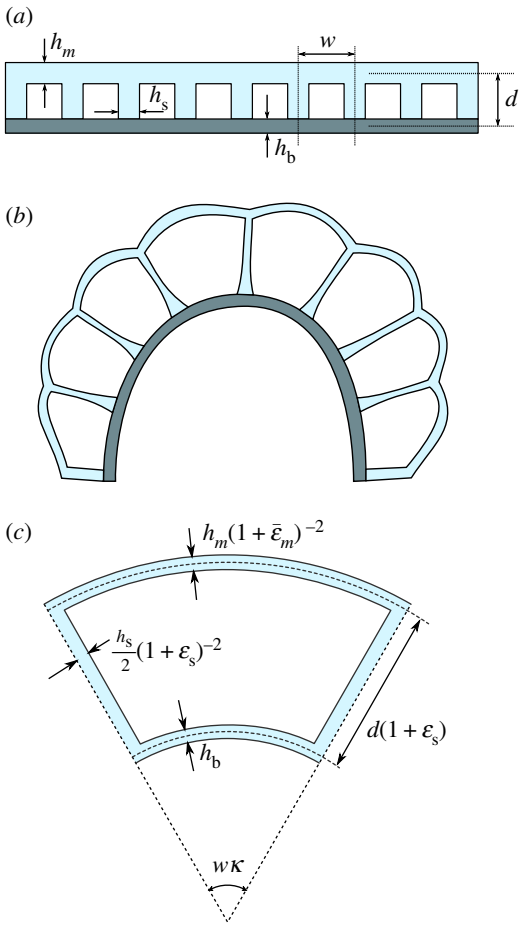

Figure 1. (*a*) Schematic diagram of the actuator geometry indicates the chamber dimensions and wall thicknesses. The out-of-plane dimension t is not shown. (*b*) As the actuator is inflated, the top and side walls extend, whereas the base does not. This causes the device to curve. (*c*) Geometry of the deformed chamber according to the simple concentric-circles one-chamber model of the pneu-net. (Online version in colour.)

Here, we show that, by varying the geometry and material properties of soft actuators, it is possible to natively emulate complex closed-loop control functions without requiring either sensing or external control [20,21]. In §2, we describe the pneu-net actuator and introduce a simple two-dimensional model whose predictions compare well with experimental studies. In §3, using this model, we show that soft actuators provide an excellent combination of large intrinsic compliance and significant interaction force, and that they are therefore ideal candidates for all the applications where manipulators have to interact with soft, fragile or uncertain objects. In particular, we show that the response of these actuators automatically switches between position control (for stiff objects) and force control (for soft objects), without sensing and feedback, thus resolving a major issue of object manipulation with stiff graspers. In §4, we discuss the impact of material properties and geometry on the macroscopic behaviour of the actuator, and conclude in §5 with a general principle for the design of intrinsically impedance-controlled actuators.

2. Pneu-net geometry and mechanics

In its simplest form, a pneu-net is a long trunk-like structure with a series of connected internal chambers which, when inflated pneumatically, cause the structure to transform into a curved configuration (figure 1). It has recently been proposed

as a flexible platform for robotic surgery and rehabilitation [22], and other examples where interaction with soft tissues plays a major role. The material components underlying the geometric structure are a soft and highly stretchable elastomer which is attached to a thin flat sheet of polydimethylsiloxane (PDMS). This PDMS layer is much stiffer than the first elastomer, and thus constrains one face of the device as its other faces expand. This strain mismatch in turn forces the inflated actuator to adopt a curved state.

The response of the actuator is characterized by the curvature κ of the PDMS base as a function of the inflation pressure p. For small inflation pressures, the increase in curvature of such devices is small. However, at a critical pressure, the top walls of the chambers undergo a classical ballooning instability [23–25], causing a significant jump in curvature on additional inflation. Subsequent increases in pressure have little effect on the curvature, owing to significant strain stiffening in the compliant elastomer. To understand this behaviour, we must thus account for both the geometry of the structure, which includes large rotational deformations induced by strain mismatch between the constituent materials, as well as the accompanying strain stiffening at high strains. Therefore, simple theories, such as those associated with the onset of classical ballooning, do not provide a satisfactory description of the system behaviour. On the other hand, a full three-dimensional, geometrically accurate model (like the ones presented in [26,27], for example) is insufficiently flexible to allow us to gain a fundamental understanding of the behaviour of the actuator. Instead, we need a model that is simple enough for semi-analytical manipulation while realistic enough to capture both the geometric and material nonlinearities inherent in the mechanical response of the materials in the pneu-net. One such model, predicated on the eventual inextensibility of long polymer chains, is the incompressible Gent model [28], described by a stored energy density that is given by

$$W = -\frac{\mu J}{2}\log\left(1 - \frac{(I_1 - 3)}{J}\right), \tag{2.1}$$

where I_1 is the first invariant of the left Cauchy–Green deformation tensor. This minimal model for neo-Hookean materials exhibits strain stiffening, and is consistent microscopically with the statistical mechanics of a freely jointed polymer filament. It depends on only two parameters to capture the mechanical response over a large range of strains; μ is the shear modulus (for small strains) and J is the limiting value of $I_1 - 3$ at which the material becomes infinitely stiff.

Using this material model, we consider a two-dimensional pneu-net whose deformation in the third dimension is set by empirically assuming that the elastomer wall strains are equibiaxial. Although simplified, such a model is capable of correctly capturing the actuator behaviour described in the literature [17,18]. The actuator geometry is sketched in figure 1*a*: the pneu-net is composed of a series of N chambers each having width w and height d, measured to the centre-surface of the chamber walls. The thicknesses of the top, side and base walls are denoted by, respectively, h_m, h_s and h_b. The out-of-plane depth of the actuator is denoted by t. We consider the mechanics of a single chamber, the unit cell of a pneu-net, and assume that the top and the base walls sit on concentric circles (figure 1*c*). The benefit of this configuration is that the actuator behaviour can now be described using only two parameters: the strain in the side wall ε_s, and the curvature κ of the bottom wall. Under this assumption, the strain in the top wall may be written

$$\bar{\varepsilon}_m = d(1 + \varepsilon_\mathrm{s})\kappa. \tag{2.2}$$

The actuator inflates under the application of an internal pressure difference p between the chamber and the ambient medium. At equilibrium, the pneu-net has a configuration that minimizes the total potential energy

$$U = U_\mathrm{p} + U_\mathrm{b}^b + U_\mathrm{s}^s + U_\mathrm{s}^m + U_\mathrm{obj}. \tag{2.3}$$

In this expression, U_p is the work done by the pressure p, U_b^b is the bending energy for the base, U_s^s and U_s^m represent, respectively, the stretching energy of the side and top walls, and U_obj is the potential energy stored in the grasped object. We have neglected the bending energy in the top walls as these elements are primarily loaded in tension and are much softer and more flexible than the base. Similarly, two adjacent chambers have the same internal pressure; therefore, the side walls do not undergo significant bending, and the bending energy in these elements can be neglected as well. The work done by the pressure p is simply

$$U_\mathrm{p} = -p\Delta V, \tag{2.4}$$

where ΔV is the change in the chamber volume. Taking into account the geometry and the thinning of the walls (see the electronic supplementary material), U_p can be written

$$\begin{aligned} U_\mathrm{p} = -pt\Bigg\{ & \frac{w\kappa(1+\varepsilon_\mathrm{s})}{2}\left[d(1+\varepsilon_\mathrm{s}) - \frac{h_\mathrm{m}}{2(1+\bar{\varepsilon}_m)^2} - \frac{h_\mathrm{b}}{2}\right] \\ & \times\left[d(1+\varepsilon_\mathrm{s}) - \frac{h_\mathrm{m}}{2(1+\bar{\varepsilon}_m)^2} - \frac{h_\mathrm{s}(\cot w\kappa + \operatorname{csc} w\kappa)}{(1+\varepsilon_\mathrm{s})^2}\right. \\ & \left. + \frac{h_\mathrm{b}}{2} + \frac{2}{\kappa}\right] - (w - h_\mathrm{s})\left(d - \frac{h_\mathrm{b}}{2} - \frac{h_\mathrm{m}}{2}\right)\Bigg\}. \end{aligned} \tag{2.5}$$

The remaining terms in the energy can be approximated by

$$U_\mathrm{b}^b = \frac{E_\mathrm{b} h_\mathrm{b}^3 \kappa^2 wt}{24(1-\nu^2)}, \tag{2.6}$$

$$U_\mathrm{s}^s = -\frac{\mu J dth_\mathrm{s}}{2}\log\left(1 - \frac{(I_1(\varepsilon_\mathrm{s}) - 3)}{J}\right), \tag{2.7}$$

$$U_\mathrm{s}^m = -\frac{\mu J wth_\mathrm{m}}{2}\log\left(1 - \frac{(I_1(\bar{\varepsilon}_m) - 3)}{J}\right) \tag{2.8}$$

and

$$U_\mathrm{obj} = wtW_\mathrm{obj}, \tag{2.9}$$

where W_obj is the elastic energy stored in the object per unit contact area and

$$I_1(\varepsilon) = 2(1+\varepsilon)^2 + (1+\varepsilon)^{-4}, \tag{2.10}$$

owing to the equibiaxial extension assumption.

For simplicity, we assume that the pneu-net is used to grasp a soft object along a circular arc of radius $1/\kappa_\mathrm{obj}$ with a uniform local spring stiffness k_obj. If the normal displacement associated with the pneu-net contacting the object is $1/\kappa_\mathrm{obj} - 1/\kappa$, we may write the elastic energy stored in the object per unit area as

$$W_\mathrm{obj} = \begin{cases} \dfrac{k_\mathrm{obj}}{2\kappa^2\kappa_\mathrm{obj}^2}(\kappa - \kappa_\mathrm{obj})^2 & \text{if } \kappa > \kappa_\mathrm{obj}, \\ 0 & \text{if } \kappa < \kappa_\mathrm{obj}. \end{cases} \tag{2.11}$$

This is equivalent to setting $k_\mathrm{obj} = 0$ when $\kappa < \kappa_\mathrm{obj}$, i.e. when the object is not grasped.

Minimizing the total energy of the pneu-net and the object yields the equilibrium configuration of the system and sets the stage for understanding its potential use as a robotic element.

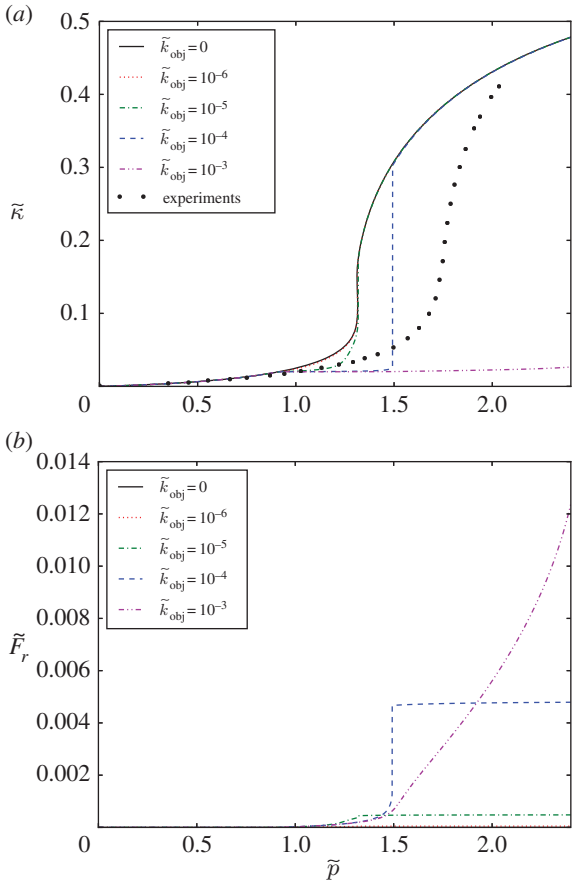

Figure 2. Plots display the variation in (*a*) dimensionless curvature $\tilde{\kappa} = w\kappa$. For qualitative comparison, we also plot (dotted line) the experimental variation in curvature for a class of pneu-nets [27], which shows similar behaviour (*b*) dimensionless applied force $\tilde{F}_r = \mu F_r$ as the dimensionless pressure $\tilde{p} = p/\mu$ varies, for five different values of the dimensionless object stiffness $\tilde{k}_{obj} = w\mu^{-1}k_{obj}$. Solutions were found for representative parameter values $d = w = h_m = h_s = 2h_b$, $E_b = 60\mu$, $\nu = \frac{1}{2}$, $J = 15$ and $\kappa_{obj} = (50w)^{-1}$. (Online version in colour.)

3. Autonomous intrinsic impedance control

To understand the grasping performance of pneu-nets, we ask how the force used to grasp objects varies as a function of the stiffness of the grasped object relative to that of pneu-net itself, noting that the stiffness of the pneu-net is itself a function of both its material properties and its geometry. To evaluate the applied force (per unit length) on the object, we minimize (2.3) for several different values of k_{obj} and for incrementally increasing values of p, and determine

$$F_r = k_{obj}\left(\frac{1}{\kappa_{obj}} - \frac{1}{\kappa}\right). \tag{3.1}$$

In figure 2*a*,*b*, we plot the curvature κ and the applied force F_r as functions of increasing pressure and the dimensionless stiffness of the grasped object $k_{obj}w/\mu$. We clearly see two different characteristic actuator behaviours; for very compliant objects ($k_{obj} \lesssim 10^{-6}\mu/w$), the pressure–curvature graph in figure 2*a* is almost coincident with that of the object-free actuator. This leads to a gradual increase in curvature for low pressures, followed by a rapid increase at a critical pressure, and subsequently a saturation to a constant curvature owing to the strain-stiffening behaviour of the elastomer. This observation is in qualitative agreement with experimental results reported in [17,18,27]. For comparison, in figure 2*a*, we plot a recent pressure–curvature curve reported in [27] for a five-chambered device with comparable dimensions, and see that our minimal model can capture the salient features of the observations despite the many simplifications we have made. In figure 2*b*, we also see that the applied force per unit width increases as the balloon instability gets underway, but for larger pressures the applied force saturates to a constant value when the scaled stiffness of the grasped object is very small.

Conversely, in figure 2*a*,*b*, we see that, for very stiff objects ($k_{obj} \gtrsim 10^{-3}\mu/w$), the curvature of the pneu-net coincides approximately with that of the grasped object, whereas the applied force increases monotonically as the pressure in the actuator is increased. We see that the grasper thus automatically switches from position to force control as the grasped object stiffness changes; for soft objects the force applied to the object is constant, whereas for stiff objects the displacement of the actuator (represented by κ) is constant. These two limits are precisely what is required of an impedance-controlled device, except that here they arise naturally in the absence of any sensing or feedback control. The transition between force and position control occurs at intermediate values of $k_{obj}w/\mu$.

When the actuator is in contact with an arbitrary object, as the pressure increases, the curvature of the actuator increases until it coincides with the curvature of the grasped object. For a subsequent increase in the pressure, the curvature of the actuator is slaved to that of the object, while the force increases. Eventually, at a certain value of the pressure (not necessarily related to that of the balloon instability) the grasped object gives in to the actuator, and subsequently becomes very soft, allowing the actuator curvature to change as if it were not grasping anything, until the applied force saturates at a constant value. To couch these notions in a concrete example, let the grasped object be a curved arc of outer radius $r_1 = \kappa_{obj}^{-1}$, thickness H, and made of an incompressible material with shear modulus μ_{obj}. The Winkler elastic constant of this object can then be shown to be

$$k_{obj} = 2\mu_{obj}\kappa_{obj}\left[\frac{1}{(1 - H\kappa_{obj})^2} - 1\right] \tag{3.2}$$

(see electronic supplementary material). Following [17,18], we consider a typical object thickness $H = 1$ cm (comparable to the thickness of the actuators), and let the elastomer have shear modulus 50 kPa and chamber width 5 mm. Then, using the parameter choices in figure 2, the object stiffness can be related to $\tilde{k}_{obj}$ through

$$\mu_{obj} \sim (1.5 \times 10^7 \tilde{k}_{obj})\ \text{Pa}. \tag{3.3}$$

Thus a stiff object of shear modulus 15 kPa or more ($\tilde{k}_{obj} \geq 10^{-3}$), such as an elastomer, would be grasped by this actuator without being deformed, though the traction on the object would increase unboundedly with increasing pressure. Conversely, a compliant object, such as a gel or foam with shear modulus less than 1.5 kPa ($\tilde{k}_{obj} < 10^{-4}$), would undergo large deformations while being grasped, though the tractions it experienced would be bounded.

4. General criteria for actuator design

Even in our minimal model, the effective stiffness of the pneu-net developed in §2 is seen to be a function of its geometry and material properties, both of which can be varied to affect its

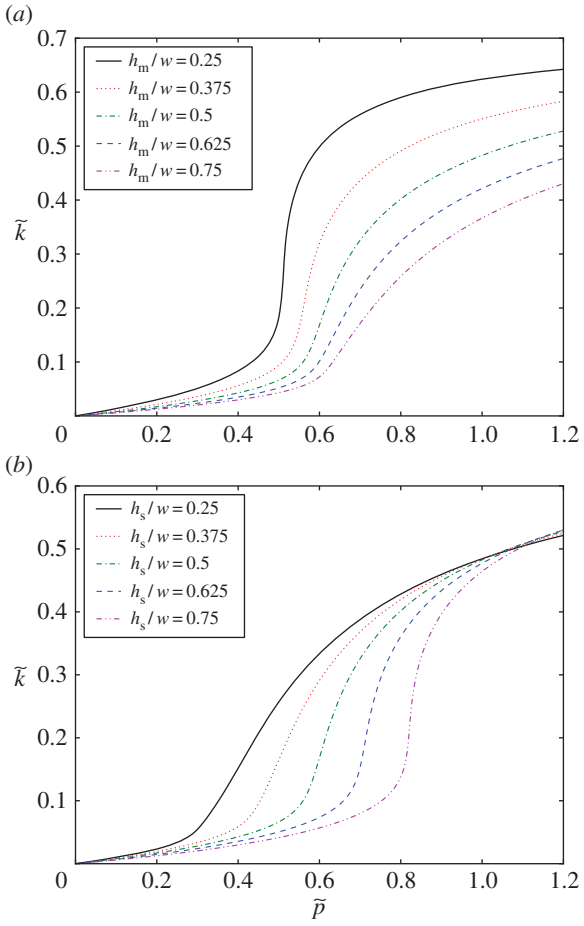

Figure 3. Graphs of the dimensionless pressure–curvature relation of the actuator, changing one geometric or material parameter while keeping others fixed. (*a*) The top wall thickness h_m/w. (*b*) The side wall thickness h_s/w. Apart from these, parameter values are fixed at $h_b = h_m = h_s = d/2 = w/2$, $E_b = 60\mu$, $\nu = \frac{1}{2}$, $J = 20$, $k_{obj} = 0$. The dimensionless pressure is $\tilde{p} = p/\mu$, whereas the dimensionless curvature is $\tilde{\kappa} = w\kappa$. (Online version in colour.)

macroscopic response. Variations in material parameters (achieved by altering the curing process or using a different type of elastomer) and chamber geometry can thus be successfully exploited to tailor the shape of the pressure–curvature graph and thence the design of the actuator to different requirements dictated by specific grasping applications.

There are four characteristics of this pressure–curvature relation that can be modified by changing these parameters: (i) the initial slope, which is a measure of actuator stiffness; (ii) the critical pressure at which the ballooning instability occurs, which determines the location of abrupt transition in the actuator stiffness; (iii) the severity of this instability, i.e. the maximum gradient in the pressure–curvature response relation; and (iv) the maximum curvature achieved after strain stiffening. Figure 3 shows the results of varying the wall thicknesses h_m and h_s on these characteristics, while keeping all of the other constants fixed (see the electronic supplementary material for the dependence on the other parameters). We find that the critical pressure for initiation of the balloon instability is very sensitive to changes in the parameters; the instability can be made to occur at a lower pressure by lowering the value of μ, the wall stiffness, or as a result of lowering the wall thickness h_m or h_s relative to the chamber width w. In either case, this corresponds to a weakening of the chamber walls and leads to an aneurysm.

More generally, our analysis shows that we can control the severity of the balloon instability by varying the geometric parameters at our disposal. For example, if we need a fine-grained control over the curvature, having a sudden jump in the curvature as the actuator pressure passes a critical value can be deleterious. Instead, we can smooth this jump by lowering the Gent parameter J (see electronic supplementary material). This has the effect of lowering the strain at which strain stiffening occurs, making the curvature jump smaller. Conversely, increasing J allows the actuator to reach larger curvatures, but it may 'snap' owing to transient instabilities where the geometric softening is not suitably counterbalanced by strain stiffening. The jump in the pressure–curvature graph may also be mollified by stiffening the top wall (by increasing h_m), or by *weakening* the side wall (by reducing h_s). The latter is effective because it allows more of the work done by pressure to be stored in the side walls rather than in the top wall, where the balloon instability has its effect.

5. Discussion

Building on experimental observations of pneu-nets for grasping [17], locomotion [18] and generic actuation [19], we have derived a simple theoretical model for these actuators to show that they are particularly suitable for robotic grasping in the presence of mechanical and geometric uncertainty in graspable objects. Furthermore, their intrinsically large compliance allows them to interact with the environment without requiring an additional feedback controller, efficiently solving many of the problematic issues associated with traditional hard robotic manipulation. In particular, the geometrically nonlinear effects that take over once the actuator is in contact with an object allow for stable grasping of objects with intrinsically small stiffnesses. This is because in pneu-nets large compliance does not necessarily translate to low values of the interaction force, this being regulated by the inflation pressure p.

From a mathematical and engineering perspective, pneu-nets are thus capable of intrinsic impedance control, without a sophisticated sensing and control strategy. This desirable feature is a direct consequence of the ability of pneu-nets to provide two different pathways for expending the work done by the inflation pressure: (i) object deformation and (ii) actuator deformation. When grasping compliant objects, most of the work is done to deform the object, just as in standard rigid actuators in the limit of position control. On the other hand, when grasping stiff objects most of the energy is spent on deforming the actuator itself, leading to force control. We note that this latter option is precluded in the standard design of rigid actuators that do not have the ability to store internal energy in self-deformation. This simple observation provides a general design principle for actuators with autonomous intrinsic impedance control: any potential design must provide at least two different ways of expending the energy provided by the control input. While pressure-driven soft actuators satisfy this criterion, other designs that have the flexibility to vary both conjugate components of work will also be feasible.

From a design perspective, this general principle can be used as guidance for designing new actuators capable of 'morphological computation' or passive control of the interaction with an unknown environment. Besides obvious

applications in human–robot interaction, medicine and rehabilitation (as suggested, for example, in [22]), such a capability has the potential to have an impact in a variety of industrial settings such as agriculture and food handling [29].

From a broader evolutionary perspective, the presence of soft structures in many biological situations that deal with geometric and mechanical uncertainty in the environment points to a natural convergence of a design that allows for intrinsic impedance control. Our theoretical study shows that pneu-nets, or similar soft slender fluidically actuated structures, reduce the demands on a complex central controller by harnessing the local link between force and deformation via geometric and material nonlinearities and obviate the need for sensing and feedback control. This simple fact might well have driven their near ubiquitous presence in early metazoans [14].

Authors' contributions. P.P., G.W.J and L.M. conceived the study and developed the model. P.P. and G.W.J. did the calculations. P.P., G.W.J and L.M. wrote the paper.

Competing interests. We declare we have no competing interests.

Funding. We acknowledge partial financial support from NSF DMR 14-20570 (L.M.), ARO W911NF-15-1-0166 (L.M.) and NSF DMREF 15-33985 (L.M.).

References

1. Lewis FL, Dawson DM, Abdallah CT. 2004 *Robot manipulator control: theory and practice*, 2nd edn. Control Engineering Series, vol. 15. New York, NY: Marcel Dekker.
2. Ma RR, Spiers A, Dollar AM. 2016 M2 gripper: extending the dexterity of a simple, underactuated gripper. In *Advances in reconfigurable mechanisms and robots II* (eds X Ding, X Kong, JS Dai). Mechanisms and Machine Science, vol. 36, pp. 795–805. Cham, Switzerland: Springer International Publishing.
3. Hogan N. 1984 Impedance control: an approach to manipulation. In *Proc. the American Control Conf., San Diego, CA, 6–8 June 1984*, pp. 304–313. New York, NY: IEEE.
4. Chiaverini S, Siciliano B, Villani L. 1999 A survey of robot interaction control schemes with experimental comparison. *IEEE/ASME Trans. Mechatronics* **4**, 273–285. (doi:10.1109/3516.789685)
5. Kim B-H, Yi B-J, Oh S-R, Suh IH. 2003 Independent finger and independent joint-based compliance control of multifingered robot hands. *IEEE Trans. Robot. Autom.* **19**, 185–199. (doi:10.1109/TRA.2003.808846)
6. Bonilla I, Reyes F, Mendoza M, González-Galván EJ. 2011 A dynamic-compensation approach to impedance control of robot manipulators. *J. Intell. Robot. Syst.* **63**, 51–73. (doi:10.1007/s10846-010-9476-x)
7. Kim S, Laschi C, Trimmer B. 2013 Soft robotics: a bioinspired evolution in robotics. *Trends Biotechnol.* **31**, 287–294. (doi:10.1016/j.tibtech.2013.03.002)
8. Laschi C, Cianchetti M. 2014 Soft robotics: new perspectives for robot bodyware and control. *Front. Bioeng. Biotechnol.* **2**, 3. (doi:10.3389/fbioe.2014.00003)
9. Rus D, Tolley MT. 2015 Design, fabrication and control of soft robots. *Nature* **521**, 467–475. (doi:10.1038/nature14543)
10. Laschi C. 2015 Soft robotics research, challenges, and innovation potential, through showcases. In *Soft robotics* (eds A Verl, A Albu-Schäffer, O Brock, A Raatz), ch. 21, pp. 255–264. Berlin, Germany: Springer.
11. Mason MT, Rodriguez A, Srinivasa SS, Vazquez AS. 2012 Autonomous manipulation with a general-purpose simple hand. *Int. J. Robot. Res.* **31**, 688–703. (doi:10.1177/0278364911429978)
12. Dollar AM, Howe RD. 2005 Towards grasping in unstructured environments: grasper compliance and configuration optimization. *Adv. Robot.* **19**, 523–543. (doi:10.1163/156855305323383785)
13. Brown E, Rodenberg N, Amend J, Mozeika A, Steltz E, Zakin MR, Lipson H, Jaeger HM. 2010 Universal robotic gripper based on the jamming of granular material. *Proc. Natl Acad. Sci. USA*, **107**, 18 809–18 814. (doi:10.1073/pnas.1003250107).
14. Clark RB. 1964 *Dynamics in metazoan evolution*. Oxford, UK: Oxford University Press.
15. Laschi C, Cianchetti M, Mazzolai B, Margheri L, Follador M, Dario P. 2012 Soft robot arm inspired by the octopus. *Adv. Robot.* **26**, 709–727. (doi:10.1163/156855312X626343)
16. Saunders F, Trimmer BA, Rife J. 2011 Modeling locomotion of a soft-bodied arthropod using inverse dynamics. *Bioinspir. Biomim.* **6**, 016001. (doi:10.1088/1748-3182/6/1/016001)
17. Ilievski F, Mazzeo AD, Shepherd RF, Chen X, Whitesides GM. 2011 Soft robotics for chemists. *Angew. Chem. Int. Ed.* **50**, 1890–1895. (doi:10.1002/anie.201006464)
18. Shepherd RF, Ilievski F, Choi W, Morin SA, Stokes AA, Mazzeo AD, Chen X, Wang M, Whitesides GM. 2011 Multigait soft robot. *Proc. Natl Acad. Sci. USA* **108**, 20 400–20 403. (doi:10.1073/pnas.1116564108)
19. Martinez RV, Fish CR, Chen X, Whitesides GM. 2012 Elastomeric origami: programmable paper-elastomer composites as pneumatic actuators. *Adv. Funct. Mater.* **22**, 1376–1384. (doi:10.1002/adfm.201102978)
20. Pfeifer R, Gómez G. 2009 Morphological computation—connecting brain, body, and environment. In *Creating brain-like intelligence* (eds B Sendhoff, E Körner, O Sporns, H Ritter, K Doya). Lecture Notes in Computer Science, vol. 5436, pp. 66–83. Berlin, Germany: Springer.
21. Nakajima K, Li T, Hauser H, Pfeifer R. 2014 Exploiting short-term memory in soft body dynamics as a computational resource. *J. R. Soc. Interface* **11**, 20140437. (doi:10.1098/rsif.2014.0437)
22. Polygerinos P, Wang Z, Galloway KC, Wood RJ, Walsh CJ. 2015 Soft robotic glove for combined assistance and at-home rehabilitation. *Robot. Auton. Syst.* **73**, 135–143. (doi:10.1016/j.robot.2014.08.014)
23. Mallock A. 1890 Note on the instability of India-rubber tubes and balloons when distended by fluid pressure. *Proc. R. Soc. Lond. A* **49**, 458–463. (doi:10.1098/rspl.1890.0116)
24. Gent AN. 2005 Elastic instabilities in rubber. *Int. J. Non-Linear Mech.* **40**, 165–175. (doi:10.1016/j.ijnonlinmec.2004.05.006)
25. Kanner LM, Horgan CO. 2007 Elastic instabilities for strain-stiffening rubber-like spherical and cylindrical thin shells under inflation. *Int. J. Non-Linear Mech.* **42**, 204–215. (doi:10.1016/j.ijnonlinmec.2006.10.010)
26. Mosadegh B *et al.* 2014 Pneumatic networks for soft robotics that actuate rapidly. *Adv. Funct. Mater.* **24**, 2163–2170. (doi:10.1002/adfm.201303288)
27. Moseley P, Florez JM, Sonar HA, Agarwal G, Curtin W, Paik J. 2016 Modeling, design, and development of soft pneumatic actuators with finite element method. *Adv. Eng. Mater.* **18**, 978–988. (doi:10.1002/adem.201500503)
28. Gent AN. 1996 A new constitutive relation for rubber. *Rubber Chem. Technol.* **69**, 59–61. (doi:10.5254/1.3538357)
29. Rossiter J, Hauser H. 2016 Soft robotics—the next industrial revolution?. *IEEE Robot. Autom. Mag.* **23**, 17–20. (doi:10.1109/MRA.2016.2588018)

Supporting information for "Grasping with a soft glove: intrinsic impedance control in pneumatic actuators"

P Paoletti, GW Jones, L Mahadevan

1 Justification for the expression for ΔV

In the article we required the expression for the change in volume for one chamber under the assumption that its top and bottom walls lie on concentric circles. Representing the pre-inflation volume by V_0 and the post-inflation volume by V_1, we have $\Delta V = V_1 - V_0$. Before inflation, the chamber has dimensions in the x, y and z directions of w, d, and t respectively. The thickness of the side, top, and bottom walls pre-inflation are respectively h_s, h_m and h_b. Thus the original volume of the cavity is

$$V_0 = t(w - h_s)\left(d - \frac{h_b}{2} - \frac{h_m}{2}\right). \tag{1}$$

Following inflation, the thicknesses of the side and top walls are reduced to $h_s(1+\varepsilon_s)^{-2}$ and $h_m(1+\bar{\varepsilon}_m)^{-2}$ respectively, where ε_s and $\bar{\varepsilon}_m$ are the respective strains in the walls. The geometry of the deformed cavity is shown in Figure 1, and its cross-sectional area can be seen to be the difference of two circular sectors, so

$$\Delta S = S_{r_1+r_2,w\kappa} - S_{r_1,w\kappa}, \tag{2}$$

where $S_{r,\theta} = \theta r^2/2$ is the area of the circular sector with radius r and angle θ. Multiplying this area difference by the assumed out-of-plane cavity length $t(1+\varepsilon_s)$ (due to the equibiaxial strain assumption in the side wall), we find

$$V_1 = \frac{tw\kappa(1+\varepsilon_s)}{2}\left[(r_1+r_2)^2 - r_1^2\right] \tag{3}$$

$$= \frac{tw\kappa(1+\varepsilon_s)}{2} r_2(r_2+2r_1). \tag{4}$$

From Figure 1, r_2 is the vertical height of the deformed cavity while r_1 is largely the radius of curvature of the bottom wall, but corrected for the finite thickness of the bottom wall and a correction factor λ due to the thickness of

the side wall:

$$r_1 = \frac{h_b}{2} + \frac{1}{\kappa} - \lambda, \tag{5}$$

$$r_2 = d(1+\varepsilon_s) - \frac{h_m}{2}(1+\bar{\varepsilon}_m)^{-2} - \frac{h_b}{2}, \tag{6}$$

so that

$$V_1 = \frac{tw\kappa(1+\varepsilon_s)}{2}\left[d(1+\varepsilon_s) - \frac{h_m}{2}(1+\bar{\varepsilon}_m)^{-2} - \frac{h_b}{2}\right] \times \left[d(1+\varepsilon_s) - \frac{h_m}{2}(1+\bar{\varepsilon}_m)^{-2} + \frac{h_b}{2} + \frac{2}{\kappa} - 2\lambda\right]. \tag{7}$$

To determine the length λ geometrically (see inset to Figure 1), we see that the length λ can be written as $\ell_1 + \ell_2$, where ℓ_1 is the edge length of rhombus A. Both ℓ_1 and ℓ_2 can be determined from the right triangle B, where L is half the thickness of the side wall, $L = h_s(1+\varepsilon_s)^{-2}/2$:

$$\ell_1 = L\csc w\kappa, \qquad \ell_2 = L\cot w\kappa, \tag{8}$$

$$\Rightarrow \quad \lambda = L(\csc w\kappa + \cot w\kappa), \tag{9}$$

and thus

$$V_1 = \frac{tw\kappa(1+\varepsilon_s)}{2}\left[d(1+\varepsilon_s) - \frac{h_m}{2}(1+\bar{\varepsilon}_m)^{-2} - \frac{h_b}{2}\right] \times \left[d(1+\varepsilon_s) - \frac{h_m}{2}(1+\bar{\varepsilon}_m)^{-2} + \frac{h_b}{2} + \frac{2}{\kappa} - h_s(1+\varepsilon_s)^{-2}(\csc w\kappa + \cot w\kappa)\right]. \tag{10}$$

2 Nondimensionalization

Representative values of the geometric and material parameters used in the model are displayed in Table 1.

The equations are solved in a dimensionless setting, using the nondimensional parameters $d/w = 1$, $h_m/w = h_s/w = h_b/w = 0.5$, $E_b/\mu = 60$, $w\kappa_{obj} = 0.02$, in addition to J and ν listed in Table 1. The chamber depth t is listed for completeness; it does not affect the solution.

3 Calculation of the Winkler elastic constant for a grasped object

We consider the grasped object to be a sector of an annulus of outer radius κ_{obj}^{-1} and inner radius $\kappa_{obj}^{-1} - H$. The Winkler elastic constant measures the traction on the outer surface of this object for a given displacement. We are not looking

Symbol	Quantity	Typical value
w	Chamber width	5 mm
d	Chamber depth	5 mm
t	Chamber out-of-plane depth	5 mm
h_b	Base PDMS layer thickness	2.5 mm
h_s	Side wall thickness	2.5 mm
h_m	Top wall thickness	2.5 mm
μ	Elastomer shear modulus	50 kPa
J	Elastomer Gent limit parameter	20
E_b	PDMS Young's modulus	3 MPa
ν	PDMS Poisson's ratio	0.5
κ_{obj}	Typical object curvature	$4\,\mathrm{m}^{-1}$

Table 1: Parameter values used for numerical calculations in this article.

to solve this problem exactly, so to get a representative value for this constant we consider the compression of a full annulus in plane strain.

An annulus with inner and outer radii r_0, r_1 respectively, on which are imposed radial tractions $-p_0$, $-p_1$, has displacement field

$$U(r) = \frac{r_1^2 p_1 - r_0^2 p_0}{r_0^2 - r_1^2} \frac{r}{2(\lambda+\mu)} + \frac{r_0^2 r_1^2 (p_1 - p_0)}{r_0^2 - r_1^2} \frac{1}{2\mu r}, \tag{11}$$

where λ, μ are the Lamé constants of the material [1]. Now assume that the traction at the interior is zero, and that the material is incompressible ($\lambda \to \infty$). Then the displacement on the outer surface is

$$U(r_1) = \frac{r_0^2 r_1 p_1}{2\mu(r_0^2 - r_1^2)} \tag{12}$$

This corresponds to a Winkler constant of

$$k_{obj} = \frac{2\mu(r_1^2 - r_0^2)}{r_0^2 r_1} \tag{13}$$

which, in terms of κ_{obj}, reads

$$k_{obj} = 2\mu\kappa_{obj}\left[\frac{1}{(1 - H\kappa_{obj})^2} - 1\right]. \tag{14}$$

4 Parameter selection criteria

In Figure 2 we plot the dimensionless curvature $\widetilde{\kappa} = w\kappa$ as a function of dimensionless inflation pressure $\widetilde{p} = p/\mu$, for a range of parameter values. We chose to vary the wall thicknesses (as a fraction of the chamber width w), the chamber aspect ratio d/w, and the Gent parameter J. Little change was observed

on varying h_b or E_b (as the overall bending stiffness is largely dominated by stretching in the top wall), and t was irrelevant in our two-dimensional model.

Analysis of these graphs shows that the actuator can be made more compliant for small pressures by increasing w, or by decreasing h_m or μ. This corresponds to a weakening of the top wall, the major contributor to the actuator's bending stiffness.

Changes in the actuator's initial stiffness can be understood by referring to the small-strain limit. We can take the full expression for potential energy, and analyze it further in the limit of small curvatures and strains, keeping only quadratic terms:

$$\begin{aligned} U_{lin} = \frac{t}{2}\Big[&- h_s p(h_b + h_m) + 2d(6h_s\mu - pw)\Big]\varepsilon_s^2 \\ &+ \frac{ptw}{8}\Big[h_b^2 - (2d + h_m)(6d + h_m)\Big]\varepsilon_s\kappa \\ &+ \frac{t}{24}\Big[E_b h_b^3 w(1-\nu^2)^{-1} + (h_b + h_m)h_s p w^2 \\ &+ 2dpw(6h_m^2 - h_s w) - 12d^2 h_m(3h_s p - 12\mu w - pw)\Big]\kappa^2 \\ &+ \frac{pt}{2}\Big[(h_b + h_m)(h_s + w) - 4dw\Big]\varepsilon_s \\ &+ \frac{pt}{8}\Big[8dh_m h_s + w(h_b^2 - (2d + h_m)^2)\Big]\kappa. \end{aligned} \quad (15)$$

This expression assumes that the object is not being grasped ($k_{obj} = 0$), and helps us understand the behavior of the system in the small-curvature (initial inflation) limit. At equilibrium, the curvature κ and side wall strain ε_s must satisfy

$$\frac{\partial U_{lin}}{\partial \kappa} = 0, \qquad \frac{\partial U_{lin}}{\partial \varepsilon_s} = 0. \quad (16)$$

This leads to a closed-form expression for the curvature in terms of the applied pressure. The leading-order behavior of this expression for small pressures p is

$$\kappa(p) \sim \frac{p(4dw(d + h_m) + (h_m^2 - h_b^2)w - 8dh_m h_s)}{8w(E_b h_b^3(1-\nu^2)^{-1}/12 + 12d^2 h_m \mu)}, \quad (17)$$

with a correction of $O(p^2)$. The bending stiffness of the actuator is given by the second derivative of the energy:

$$\begin{aligned} B = \frac{1}{tw}\frac{\partial^2 U_{lin}}{\partial \kappa_b^2} &= \frac{E_b h_b^3}{12(1-\nu^2)} + 12d^2 h_m \mu \\ &+ \frac{p}{12w}\left[(h_b + h_m)h_s w^2 + 2dw(6h_m^2 - h_s w) + 12d^2 h_m w - 36d^2 h_m h_s\right]. \end{aligned} \quad (18)$$

We can see that the curvature (17) is essentially determined by a balance between the moment generated by the pressure acting on the side walls, and the

overall actuator bending stiffness (18), which at low pressures is the sum of the intrinsic bending stiffness of the PDMS layer and a contribution from the resistance of the top wall. The range of validity of this linearized expression can be seen in Figure 3, which shows that it is a good assumption until the onset of the balloon instability, which is a nonlinear phenomenon requiring the use of the full hyperelastic model.

The critical pressure for initiation of the balloon instability was very sensitive to changes in the parameters. The instability could be made to occur at a lower pressure by weakening the walls (by lowering either μ, h_s, or h_m), or by increasing the chamber's aspect ratio (making it taller than it is wide). The severity of the balloon instability is discussed in the main text; for completeness we note that the jump in the pressure–curvature graph may be mollified by stiffening the top wall (by increasing h_m or J), or by weakening the side wall (by reducing h_s).

Finally we note that the maximum curvature at which the device saturates is also affected by the choice of parameters. In particular this maximum curvature can be increased by increasing the Gent parameter J, making the chamber wider than it is tall (by lowering d/w), or by weakening the top wall (by lowering h_m). Of course, since the dimensional curvature κ is given by $\widetilde{\kappa}/w$, the saturation curvature may also be increased by decreasing the size of the device (represented by the common lengthscale w).

References

[1] A. E. H. Love, *A Treatise on the Mathematical Theory of Elasticity*, Cambridge University Press, fourth ed., 1927.

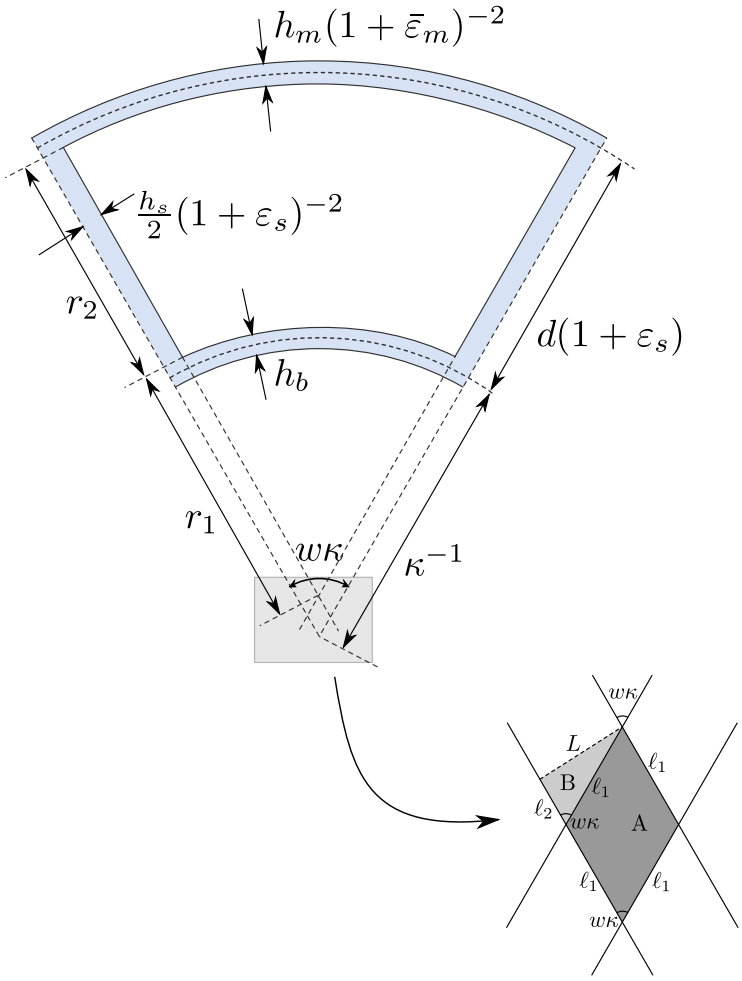

Figure 1: Schematic diagram of a pressurized chamber, modeled as a sector of an annular region.

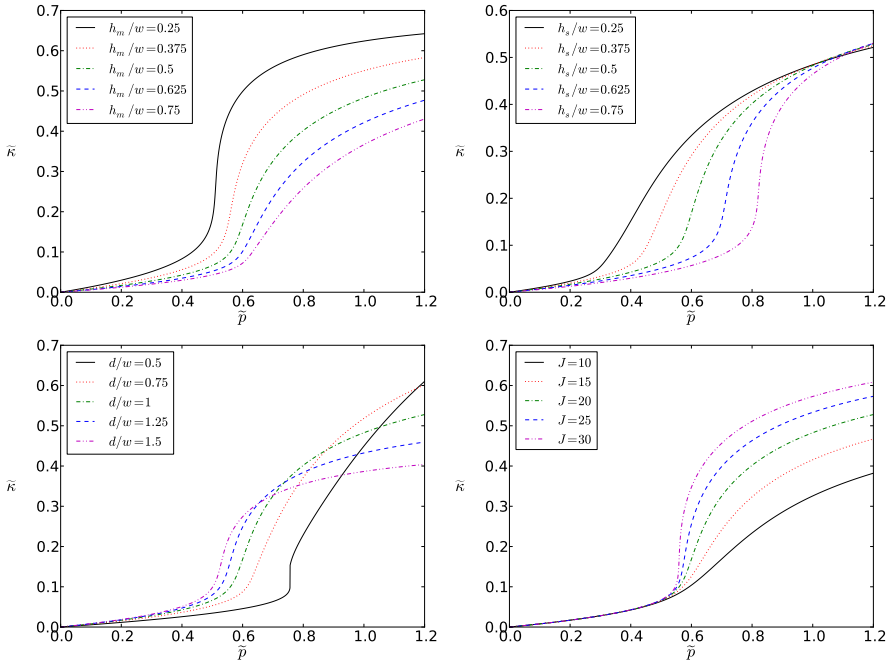

Figure 2: Graphs of the dimensionless pressure-curvature relation of the actuator, changing one geometric or material parameter while keeping others fixed. (a) The top wall thickness h_m/w. (b) The side wall thickness h_s/w. (c) The chamber aspect ratio d/w. (d) The Gent model parameter J. Apart from these, parameter values are fixed at $h_b = h_m = h_s = d/2 = w/2$, $E_b = 60\mu$, $\nu = 1/2$, $J = 20$, $k_{obj} = 0$. The dimensionless pressure is $\widetilde{p} = p/\mu$ while the dimensionless curvature is $\widetilde{\kappa} = w\kappa$.

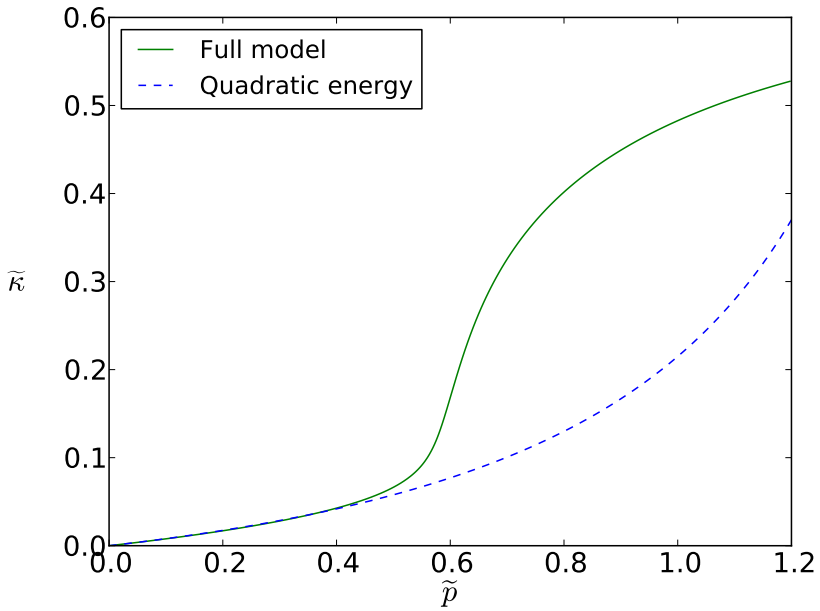

Figure 3: The dimensionless presssure–curvature relations for both the full energy minimization and the quadratic energy (15), indicating the range of validity of the latter. Parameter values are fixed at $h_b = h_m = h_s = d/2 = w/2$, $E_b = 60\mu$, $\nu = 1/2$, $J = 20$, $k_{obj} = 0$. The dimensionless pressure is $\widetilde{p} = p/\mu$ while the dimensionless curvature is $\widetilde{\kappa} = w\kappa$.